Processing of FLIR thermal images from the eruption in Grímsvötn in 2011

Sigurbjörn Bogi Jónsson

Faculty of Earth Sciences
University of Iceland
2014

Processing of FLIR thermal images from the eruption in Grímsvötn in 2011

Sigurbjörn Bogi Jónsson

10 credit ECTS thesis submitted in partial fulfillment of a *Baccalaureus Scientiarum* degree in geophysics

Advisor
Magnús Tumi Guðmundsson

Faculty of Earth Sciences
School of Engineering and Natural Sciences
University of Iceland
Reykjavík, May 2014

Processing of FLIR thermal images from the eruption in Grímsvötn in 2011
10 credit ECTS thesis submitted in partial fulfillment of a B.Sc. degree in geophysics

Faculty of Earth Sciences
School of Engineering and Natural Sciences
University of Iceland
Öskju, Sturlugötu 7
101, Reykjavík
Iceland Telephone: 525 4000

Bibliographic information:
Sigurbjörn Bogi Jónsson, 2014, *Processing of FLIR thermal images from the eruption in Grímsvötn in 2011*, B.Sc. thesis, Faculty of Earth Sciences, University of Iceland.

Printing: Háskólaprent, Fálkagötu 2, 107 Reykjavík
Reykjavík, Iceland, May 2014

Abstract

On the 21th of May 2011, explosive eruption started in Grímsvötn. To evaluate the surface temperature of the eruption plume, crater and crater lake thermal images were captured from an aircraft, on the 24th of May. In this thesis these images are analyzed and results on plume, crater and lake temperature presented. In order to get right results, the images had to be calibrated with respect to the environment, because the final temperature is a function of the following parameters: emissivity, reflected apparent temperature, atmospheric temperature, humidity, transmission and distance. A special program, FLIR ResearchIR, was used to process the data and the results were presented using graphs. The eruption's activity could be divided into three types: Continuous uprush, continuous steaming and cocktail explosions activity. Clear differences in temperature can be observed between these different types of activity. The average temperature for the uprush activity was around 20°C, for the steaming activity around 8°C and over 45°C for the cocktail explosion activity. The crater's rim was mostly under 0°C but obtained its highest temperature, around 5°C to 15°C, on the NE side. The lake could be divided in two areas. On the east side, no volcanic activity was present causing the lake's temperature to be around zero degrees. On the west side however, lots of activity was present causing the mean temperature of the lake in that area to be around 25°C. A lot of energy is needed to boil external waters, but total cooling effects from the melting, water heating and the evaporation is the main cause for lower temperature values in these plumes compared to plumes in areas with no water.

Útdráttur

Þann 21. maí 2011 hófst sprengigos í Grímsvötnum. Til að meta yfirborðshitastig gosmakkar, gígs og vatnsins í gígnum voru teknar hitamyndir úr flugvél, þann 24. maí. Í þessari ritgerð eru þessar myndir skoðaðar og niðurstöður um hitastig makkar, gígs og gígvatns settar fram. Til að réttar niðurstöður fáist þurfti að kvarða myndirnar með tilliti til umhverfisins, því loka hitastigið er háð eftirfarandi breytum: eðlisgeislun, endurkastað sýndarhitastig, hitastig loftsins, raka, gegnskin og fjarlægð. Notað var sérhæft forrit, FLIR ResearchIR, við úrvinnslu gagnanna og voru niðurstöður sýndar á gröfum. Gosvirkninni var hægt að skipta upp í 3 gerðir: samfelldur gjósku- og vatnsstrókur, samfelldur gufustrókur og einstakar sprengingar. Skýr hitamunur kom fram milli þessara þriggja gerða. Meðal hitinn fyrir gjósku- og vatnstrókinn var um 20°C, fyrir gufustrókinn um 8°C og um og yfir 45°C fyrir einstöku sprengingarnar. Gígsbarmurinn var að mestu undir frostmarki en náði mestum hita, um 5°C til 15°C, á NA hliðinni. Vatninu var hægt að skipta í tvö svæði. Austan megin gætti engrar gosvirkni og því var vatnið þar í kringum frostmark. Vestan megin var hinsvegar mikil virkni og var meðalhiti vatnsins á því svæði um 25°C. Mikil orka fer í sjóða utanaðkomandi vatn, en samanlögð kælingaráhrif af ísbráðnun, vatnshitun og suðu eru aðalástæðan fyrir lægri hitatölum í þessum mökkum samanborið við þá þar sem vatn kemur ekki við sögu.

Hér með lýsi ég því yfir að ritgerð þessi er samin af mér og að hún hefur hvorki að hluta né í heild verið lögð fram áður til hærri prófgráðu.

Sigurbjörn Bogi Jónsson
kt. 270190-2359

Contents

List of Figures

List of Tables

Abbreviations

e	-	Emissivity
FLIR	-	Forward Looking Infrared Radiometer
IR	-	Infrared radiation
Matlab	-	Matrix Laboratory
ThI	-	Thermal Image

Acknowledgements

First of all, I would like to thank my advisor, Magnús Tumi Guðmundsson, for his guidance throughout this study. His knowledge of the subject was essential for the development of this thesis.

To my family and all my friends at the University I give enormous gratitude. Without them this thesis wouldn't have taken place.

Finally I would like to thank Björn Oddsson and Finnur Pálsson at the University of Iceland for allowing me to use pictures and data for this thesis.

1 INTRODUCTION

Active volcanoes emit large amount of heat into the atmosphere. By using a thermal camera, a remote sensing device, heat emissions from volcanic sites can be measured and monitored. On the 24th of May, scientists from the University of Iceland captured 49 thermal images from an aircraft of the 2011 eruption in Grímsvötn, using hand-held FLIR thermal camera. Grímsvötn is a subglacial basaltic volcano and the purpose of the measurements was to estimate the temperature distribution in the eruption plume, the crater and the crater lake.

The final temperature of a thermal image is a function of various parameters, so in order to get true results, the images must be correctly calibrated (Harris, 2013). Consequently, the images were downloaded into special software, allowing further processing of the data. The goal of this thesis is to give as good temperature results as possible for these images from Grímsvötn and thus provide a better understanding of the physical processes occurring in a basaltic phreatomagmatic eruptions.

2 STUDY AREA

Iceland is an island, located in the North Atlantic Ocean. Its tectonic position is unique, because the Mid-Atlantic ridge crosses the country and thus separates the North-American plate from the Eurasian plate. If that wasn't enough, Iceland also sits on top of a hot spot. Consequently, Iceland is very tectonically active and contains great amounts of geothermal energy, which has supported the nation's household heating throughout the years. Another consequence of Iceland's position is vast active volcanism. The divergent plate boundaries causes the formation of three volcanic belts, the Eastern, Western and Northern Volcanic Zones, which are then connected by two transform zones (Fig. 2.1a). On these three belts, most of Iceland's volcanic activity occurs (Larsen, Guðmundsson & Björnsson, 1998).

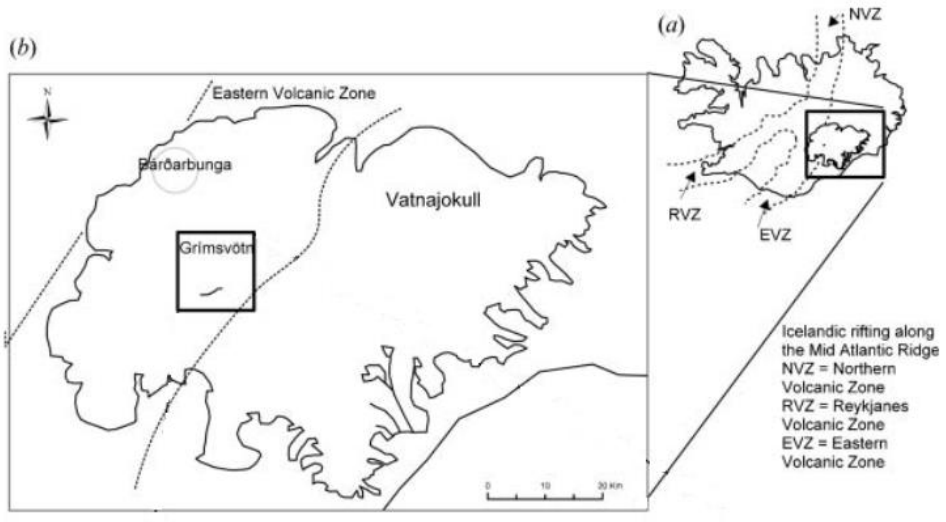

Figure 2.1: *a) Icelandic rifting along the Mid-Atlantic ridge. b) Location of Grímsvötn (from Steward et al. 2008).*

A large part of Iceland's volcanism occurs within glaciers. Subglacial eruptions usually develop into emergent phreatomagmatic eruptions, as a result of the interaction between water and magma (Jakobsson & Guðmundsson, 2008). These kinds of eruptions, also known as Surtseyan, are often associated with jökulhlaups and ash fallout and they can have devastating effects. At present time 11% of Iceland is covered by glaciers but during the last ice-age the country was almost completely ice covered (Guðmundsson, 2005). Glaciers and subglacial eruptions have therefore created and shaped the present day landscape, causing móbergs formation, tuyas and tindar which now characterize the

country (Jakobsson & Guðmundsson, 2008). This interplay between fire and ice is also an important part of the nation's history. Many historic eruptions like Laki 1783, Katla 1918 and Vestmannaeyjar 1973 are known to all Icelanders, both for the destructive effects and the beautiful scenery they left behind. Also, let's not forget about the world famous Eyjafjallajökull eruption which affected and caused cancellation and delays of flight schedules for most of Europe for days and weeks.

The most frequently erupting volcano in Iceland is Grímsvötn (Larsen et al., 1998). Grímsvötn volcano has been erupting frequently for the past millennium or on averge once every 10 years (Larsen et al., 1998). The Grímsvötn volcanic system consists of two central volcanoes, Grímsvötn and Þórðarhyrna, and an associated fissure system (Jude-Eton et al., 2012). It's located in the western part of Vatnajökull, Iceland's and Europe's largest glacier (Fig2.1b). As well as being Iceland's most active volcano, Grímsvötn is a very powerful geothermal area. This volcanism alongside the immense geothermal heat is responsible for the creation and preservation of the subglacial lake, which identifies Grímsvötn volcano. This heat is also the main cause of Grímsvötn's jökulhlaups, which occur when the caldera lake reaches an elevation sufficient enough for the meltwater to force its way under the glacier. This can lead to a 60-130 m drop in the lake level (Jude-Eton et al. 2012). Even though most eruptions are rather small (1998 and 2004), Grímsvötn can be hazardous, causing large jökulhlaups and ash emission.

2.1 Grímsvötn 2011

The latest eruption in Grímsvötn was in 2011. It started on the 21st of May and lasted for 7 days. The eruption burst out from the SW caldera rim at a similar place as the last eruption in 2004, but it was much larger in magnitude. The interaction of the basaltic magma and water resulted in a powerful exploding eruption which peaked during the first hours, with the eruption plume reaching over 20 km altitude (Hreinsdóttir et al., 2014). The following days, the plume steadily decreased. Immense ash fall followed the eruption leaving the lowlands several tens of kilometers to the south of the volcano covered in ash. The plume was mostly grayish colored but also black near the vent. Interestingly, there was a decrease in seismic activity weeks before the eruption which was very unlike the 2004 event. Only in the last hour before the onset of the eruption was there excessive seismicity (Hreinsdóttir et al., 2014). The eruption did not cause any jökulhlaups, since one had already taken place in October the year before. The magma chamber is inflating once again, so there is no doubt that Grímsvötn will erupt again in the near future (Jakobsdóttir et al., 2011).

On the 24th of May, the intensity of the eruption was much less than in the first 24 hours. Mainly two types of Surtseyan activity characterized the eruption at this time, i.e. continuous uprush and cocktail explosions activity. Continuous uprush occurs when water and magma mixture in the vent causes continuous steam and tephra plume from the crater. The term cocktail explosions describes short blast sequence activities, where large pyroclastic materials get ejected from the vent (White & Houghton, 2000). Another kind

of activity, occurring at the end of continuous uprush, was what can be called continuous steaming. This describes the case when near pure steam, without visible tephra, bursts out from the vent. Even though continuous steaming is not a specific Surtseyan type of activity, its presence is certain and it is useful for the purpose of the analysis to classify it here as a special type.

The craters were located within an ice cauldron melted out by the eruption. The cauldron was approximately 1.6 km long and 0.5-1 km wide, located in the southwest corner of Grímsvötn, under the southern caldera wall (Fig 2.2). The crater lake can be divided in two parts, the east and west side, depending on temperature where the west side is hotter than the east side.

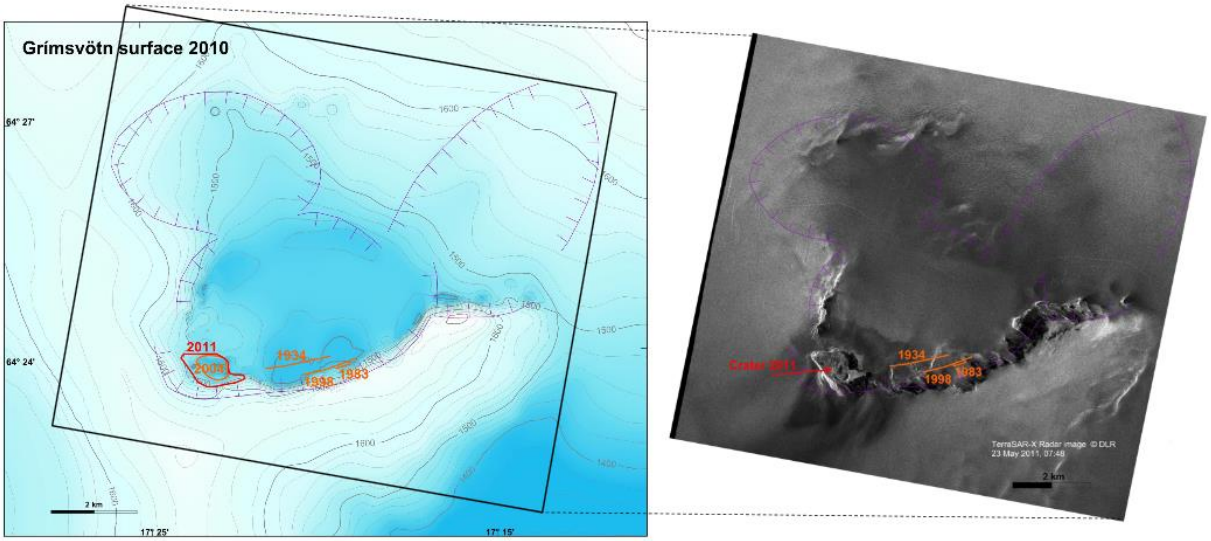

Figure 2.2*: The 2011 crater on the SW caldera rim. Crater is marked with red (from Guðmundsson et al., 2012).*

3 Thermal Imaging

Nowadays, many volcanoes are well observed and monitored. Many methods, like GPS, InSAR and seismic monitoring have been used successfully to measure Earth's deformation and assess subsurface magma flow, but to measure heat emission, plume and vent activity, other methods are required. Thermal imaging is a rather new technique which is becoming more recognizable as a tool in volcanology. Images, captured with a thermal camera, reveal temperature variations of the objects measured, which in this case are eruption sites. One of thermal imaging greatest advantages is that it is capable of covering and scanning large areas. This information can help us better understand the behavior of ash plumes, the cooling rate of lavas and give an overall information of the volcanic activity, just to name a few. Thermal imaging is based on the study of infrared radiation (IR). All objects hotter than 0 K emit infrared energy, even though we don't see it. The electromagnetic wave emitted by an object is converted into an electrical signal in a thermal camera, which then displays the temperature dependent thermal image on a monitor. But to measure the temperature correctly, several parameters must be taken into the account.

3.1 Infrared radiation

So why can't we see infrared radiation? In the same way we can't see X-rays or microwaves, the infrared rays are not part of the visible light humans can detect. The reason lies in the electromagnetic spectrum, which consists of electromagnetic waves traveling at the speed of light. All these waves transmit energy, but the difference between them is the wavelength. The electromagnetic spectrum is divided into 7 bands (Fig 3.1), from the shortest wavelength on the left (Gamma rays) to the longest on the right (Radio waves). Between the visible light and microwaves sit the infrared rays, which have wavelengths from 0.78 to 1000 μm (Young and Freedman, 2011). The infrared rays are then subdivided into three bands, the near infrared, mid infrared and far infrared band.

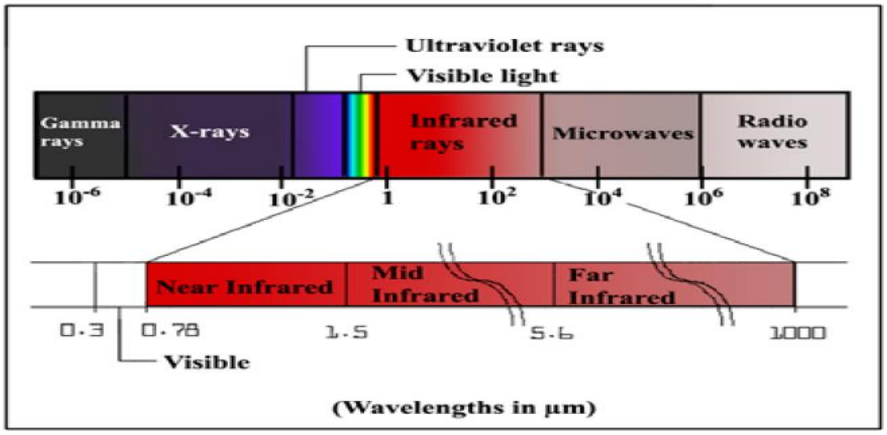

Figure 3.1*: The electromagnetic spectrum (from MikroScan 7600PRO Thermal Imager Operator's manual, 2006).*

So, even though we can't see infrared rays, all objects (hotter than absolute zero) do emit infrared radiation. Just like normal cameras capture visible light emitted from the surroundings, infrared cameras capture the emitted infrared energy. If we couldn't measure the infrared energy, there would be no thermal image. Finally, when the infrared energy has been measured then the temperature measurements can be made.

3.1.1 Emissivity

As stated earlier, to measure the temperature of a thermal image correctly, many parameters must be considered. The most important factor, regarding calibrating thermal images, is emissivity [e] (Harris, 2013). Just like visible light, infrared rays can be reflected [α], absorbed [β] or transmitted [γ] as they hit an object. The total infrared energy is the combination of these three factors, i.e.:

$$W = \alpha W + \beta W + \gamma W \tag{3.1}$$

$$\Leftrightarrow 1 = \alpha + \beta + \gamma \tag{3.2}$$

The extent to which an object reflects, absorbs or transmits IR energy is known as the emissivity of the object.

A theoretical surface which absorbs and radiates all IR energy is called a blackbody. Since all energy is absorbed ($\alpha = 0, \gamma = 0$) the blackbody's emissivity would be equal to 1. Perfect blackbodies do not exist in nature. The emissivity of an object is formally defined as the ratio between the total energy emitted by an object to that of a blackbody, at the same temperature and wavelength:

$$e = \frac{W_{object}}{W_{blackbody}} \tag{3.3}$$

Thus, the emissivity is a dimensionless number between 0 and 1. If the emissivity is 0 the object is a perfect reflector but if it is 1 the object would be a perfect emitter. The intensity of the emitted energy is a function of the temperature, so at higher temperatures the intensity of emitted IR energy is greater (Harris, 2013). Stefan-Boltzmann equation gives the correlation between the total emitted energy [W], temperature [T] and emissivity:

$$W = e \cdot \sigma \cdot T^4 \tag{3.4}$$

where σ is the Stefan-Boltzmann coefficient.

Finally, the connection between temperature and wavelength [λ] and how it affects the spectral radiant exitance [M] is given by Planck's Function:

$$M(\lambda, T) = \frac{C_1 \cdot \lambda^{-5}}{\exp\left(C_2/_{\lambda T}\right) - 1} \tag{3.5}$$

where C_1 and C_2 are spectral radiance constants (Harris, 2013).

3.1.2 Emissivity of objects relevant in volcanology

Emissivity yields best temperature values if the object measured is a surface area, i.e. water, rocks etc. But for volcanoes that's not always the case. The Surtseyan eruption plume is partially made out of ash, tephra and steam. The plume is not an ideal emissivity surface, because part of the plume's background can affect the emissivity and temperature value, since the plume is in some sense transparent. Thus, for darker plumes, containing more ash and volcanic material, the emissivity and temperature values stand closer to correct values. But for plumes containing less volcanic material, like the continuous steaming type of activity in Grímsvötn, it's harder to evaluate the correct emissivity value. The steam contains water droplets which certainly act as emissivity surfaces, but the error factor is higher.

3.2 FLIR thermal camera

There are many types of thermal cameras, but the model used for the measurements in Grímsvötn 2011 was FLIR ThermaCAM T-400 Wes (Fig 3.2). Even though thermal cameras have various features and settings they all function in a similar way. They operate in a

narrow range of the infrared radiation spectrum, usually between 7.5-14 µm (FLIR user's manual, 2008). The cameras consist of a lens, focal plane array detector, electronics and software for processing and displaying the images. The detectors can either be cooled or uncooled. The uncooled detector, as in the FLIR T-400, uses a microbolometer as a thermal sensor. As the infrared rays hit the microbolometer's material, it gets heated up and thus changes the electrical resistance of the detector. The change in the resistance is measured and processed into temperature values which make up the thermal image. The microbolometers grid consists of arrays of pixels which define the quality of the image. The detector also determines the thermal sensitivity of the image (FLIR the ultimate infrared handbook, 2008).

As stated earlier, thermal cameras have various features and settings. The list below summons up the technical specifications of the FLIR T-400 thermal camera used for 2011 Grímsvötn eruption (FLIR user's manual):

- *FOV*: 25°x19°; the field of view, or the horizontal viewing angle of the camera.
- *Detector type*: Focal Plane Array (FPA), uncooled microbolometer.
- *Thermal sensitivity*: 0.05°C @ +30°C; Noise equivalent temperature difference. This represents the minimum temperature difference which the camera can resolve. It's therefore directly related to the quality of the image, the smaller NETD gives better resolution.
- *Resolution*: 320x240 pixels.
- *Spectral range*: 7.5-13 µm.
- *IFOV*: 1.36 mRad; the instantaneous field of view . This represent the geometric resolution of the camera, i.e. the smallest object that can be viewed in the image.
- *Object temperature range*: -20°C to 120°C, 0°C to 350°C, 200°C to 1200°C. One of these options can be chosen as a setting for the camera, determined by expected target values.
- *Accuracy*: ±2°C.

The object temperature range must be chosen before using the camera. Therefore it is crucial to estimate the object temperature beforehand, because the thermal camera is less accurate outside its range. When the images have been captured, they are saved on a SD memory card as jpeg formats. These images can therefore be further processed in the FLIR ResearchIR programming software provided with the purchase of the camera.

Figure 3.2: *FLIR ThermaCAM T-400*

3.2.1 Parameters affecting thermal imaging

Even though emissivity is the most important factor regarding calibrating thermal images, other parameters also play a crucial role. The list below summarizes the parameters, other than emissivity, which can be modified in the programming software of the FLIR camera (FLIR user's manual, 2008).

- *Reflected apparent temperature [°C]*: The radiation of the measured object's surroundings, which is reflected from the object into the camera.
- *Atmospheric temperature [°C]:* The air temperature between the camera and object.
- *Relative humidity [%]*: Atmospheric humidity between the camera and object. It is presented as a number from 0 to 1, where 0 represents 0% humidity and 1 represents 100% humidity.
- *Transmission [%]*: The transmission through the atmosphere. It is presented as a number from 0 to 1, where 0 represents 0% transmission and 1 represents 100% transmission.
- *Distance [m]*: The distance between the camera and object.
- *External optics temperature*: Temperature of any external lenses in front of the camera.
- *External optics transmittance*: The transmission through any external lenses in front of the camera.

The final temperature calculation is a function of all these parameters so it is very important they are set accurately. When capturing thermal images, the camera used is pre-adjusted, meaning it is given values for the emissivity, distance etc. but these are all parameters that can be corrected for later in the FLIR ResearchIR programming software. However, what cannot be changed afterwards are the camera's fixed adjustments. Those factors must be chosen carefully before the camera is used.

3.2.2 FLIR ResearchIR

FLIR ResearchIR is the programming software from the producers of the thermal camera. Here, you can download the images and keep on processing the data, create files and add or delete images as desired. As the thermal images get downloaded into the software, the thermal image and coherent temperature scale is immediately displayed on the screen. The program automatically calculates the maximum, minimum and the mean temperature of the image and if the parameters listed in Chapter 3.2.1 are modified, the program instantly re-calculates and upgrades the temperature values. The program also offers different styles of measurement tools, like line plotting, rectangle and single measurement spots. These allow the user to measure temperature values for specific parts of the image. This also shows where the highest and lowest temperatures are located within the rectangle or on the line chosen etc. (FLIR user's manual, 2008).

When the final version of the image is complete the data can be exported, either as a jpeg image or as .csv, which allows the user to re-open the data in other programs like Excel for further processing.

4 Data

On the 24th of May, Magnús Tumi Guðmundsson and Björn Oddsson from the Institute of Earth Sciences, University of Iceland captured 49 thermal images from an aircraft at Grímsvötn. These images have running numbers from 16 to 64 and were taken over a period of 40 minutes, from 21:55 to 22:35 (uncorrected FLIR camera clock values). They mainly focused on the eruption plume, crater and the crater lake. The aircraft had only one window which could be opened (on the left hand side) and thus every thermal image was captured from the same spot on the flight. Consequently, the aircraft flew counter-clockwise around the crater, on the east and north side, since the wind direction was from the north-northeast. During the time of the flight the air temperature at 1720 m at Grímsfjall was -11.2°C (data from Finnur Pálsson). The humidity at Tungnárjökull, southwest of Grímsvötn, was measured as 63% and 93.9% for Brúarjökull, northeast of Grímsvötn. Therefore, the mean humidity value of 78% was decided for Grímsvötn (data from Finnur Pálsson). The thermal images were captured on the FLIR hand-held thermal camera but real life photos were also captured on a Canon EOS 450d camera, for comparison (see list of all images in appendix A). The cameras timer was not in sync, so every thermal image had to be manually matched with a real life image. The eruption plume was mostly light greyish colored and under 5 km altitude. The wind caused the plume to head towards SSW direction. The pictures were mostly clear and sharp, capturing various sorts of plume activity and the crater surroundings. Every image reveals Surtseyan activity but 3 types were dominant, i.e. continuous uprush, continuous steaming and cocktail explosions. Of the 49 thermal images captured, ten were either bad or out of focus so they were not used for processing. Figure 4.1 demonstrates different types of activity as well as the crater and crater lake. Finally, Table 4.2 displays the total categorization of the images, both taking the volcanic activity and plume description in account.

4.1 Parameters and errors

All images were downloaded into the FLIR ResearchIR software and once the parameters listed in Chapter 3.2.1 had been set correctly, the interpretation of the images could begin. The temperature and humidity data from an automatic weather station operating at Grímsfjall, 6 km east of the crater were provided from Finnur Pálsson at the University of Iceland. The emissivity for basaltic lava is generally between 0.9 and 0.99, with a mean of 0.95 (Harris, 2013). The emissivity value from Grímsvötn was evaluated as 0.92 which is the same value used for thermal image processing of the Eyjafjallajökull eruption in 2010 (Gridelli, 2013). Table 4.1 lists up the parameters used for every single thermal image for the Grímsvötn images, and therefore causes the final temperature results for each image.

The camera's adjusted temperature range was set from -20°C to 120°C which fitted well with the results.

The camera accuracy, according to the FLIR manual, is ±2°C. The plane was flying at around 1-4 km distance from the plume and crater so the distance factor was kept fixed at 1200 m. Of course, the plane didn't fly in fixed 1200 meters radius around the area but the effects on the final temperature are minor. As an example, for thermal image 16 (similar for every image), the temperature difference between 500 m distance and 2000 m distance is only 2.6°C.

Table 4.1: *Parameters used for the processing of every thermal image.*

Parameters	Values
Emissivity	0,92
Refl. apparent temp.	-11°C
Atmospheric temp.	-11,2°C
Relative humidity	0,78
Transmission	0,89
Distance	1200 m
External optics temp.	0°C
External optics transmission	0

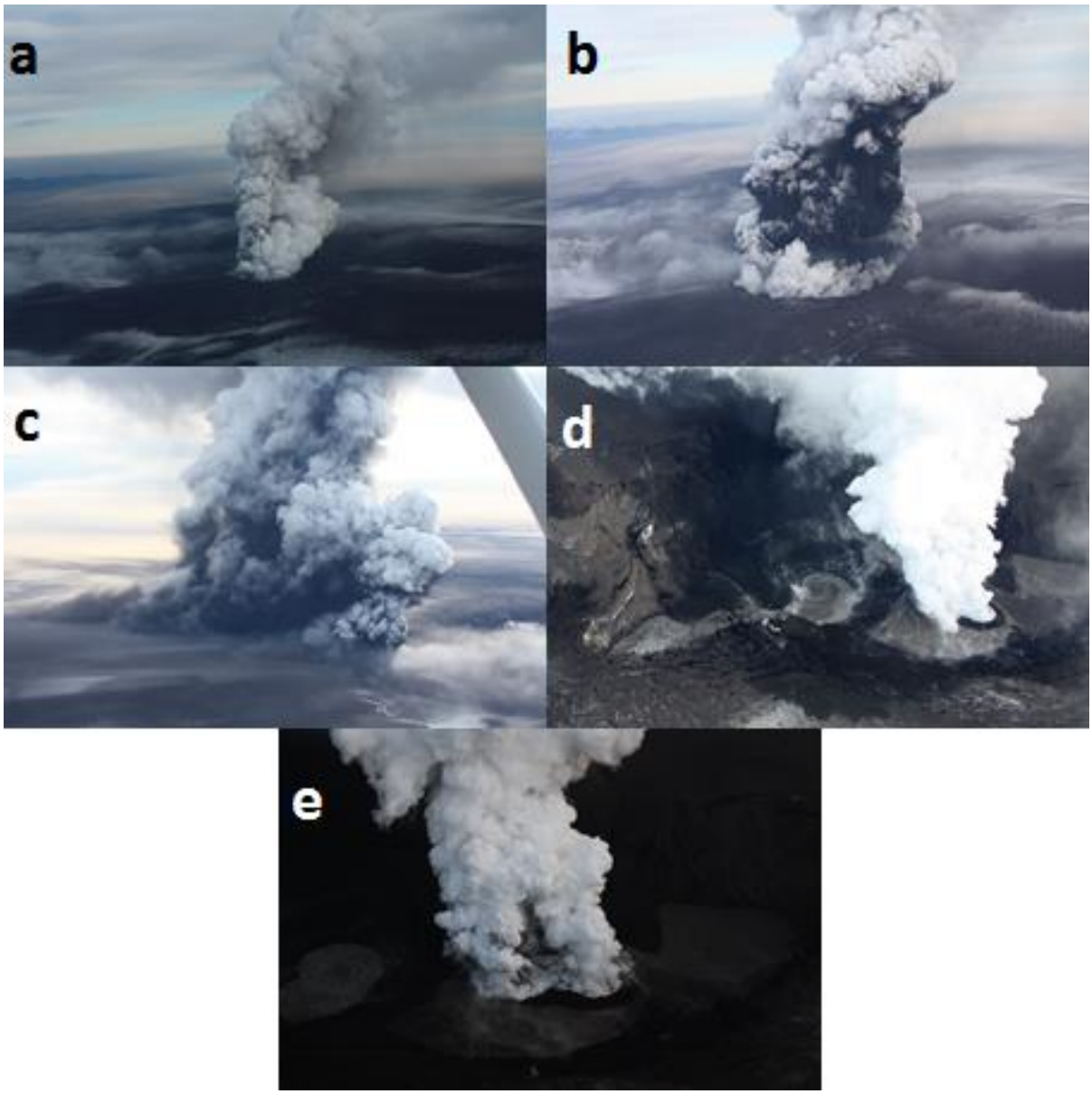

Figure 4.1: *Three types of Surtseyan activity. a) Weak continuous uprush. b) Strong continuous uprush. c) Continuous uprush associated with approximately 5 km low cloud SW of crater. d) Continuous steaming. e) Cocktail explosions near the vent and a good view of the crater (Photos by Magnús Tumi Guðmundsson)*

Table 4.2: *Categorization of the FLIR and Canon images as well as activity and plume descriptions.*

FLIR nr*.	FLIR time	Canon nr**.	Canon time	Δ t [min]	Activity	Plume
16		79	21:20	35		
17		80	21:21	34		
19	21:55	81	21:21	34	Increasing continuous uprush	light grey
20		82	21:21	34		
21		86	21:21	34		
22	21:56	88	21:23	33	Strong continuous uprush	grey to black
23		88	21:23	33		
25	22:03	137	21:29	34		
26		138	21:29	35		
27	22:04	139	21:29	35	Strong continuous uprush	grey to black, low cloud ca. 5 km SSW of crater
28		150	21:30	34		
29		151	21:30	34		
30		152	21:33	34		
31	22:07	156	21:33	34	Strong continuous uprush	black to grey, ice cauldron filled with steam
32		157	21:33	34		
33	22:13	176	21:40	33		
34		179	21:40	34		
36		180	21:40	34		
37	22:14	181	21:41	33	Continuous steaming	light grey to white
38		182	21:41	33		
39		183	21:41	33		
40		184	21:41	33		
41		205	21:43	35	Weak continuous steaming	white
42		205	21:43	35		
43	22:18	206	21:43	35		
44		218	21:47	31		
46		229	21:49	29	Weak continuous steaming	white, bottom of ice cauldron visible
47	22:19	230	21:49	30		
48		232	21:49	30		
52		245	21:52	36	Small cocktail explosions	white to light grey, plume <1 km altitude
53	22:28	246	21:52	36		
54		247	21:52	36		
56		287	22:07	26		
57	22:33	288	22:07	26		
58		289	22:07	26		
61		290	22:07	28	Small cocktail explosions	white to light grey
62	22:35	291	22:07	28		
63		292	22:07	28		
64		293	22:07	28		

*Last 2 numbers, original number: IR_2816.jpg. **Last 2-3 numbers, original number: 2011-05-24MTG79.

5 Results

As previously mentioned, the images are categorized into eruption plumes, crater and the crater lake. The data from the FLIR ResearchIR was exported as .csv file and saved as .xlsx files. From there, the data was opened with Matlab which was used to plot the graphs.

5.1 Eruption plume

The lower part of the eruption plume was visible in every single thermal image. As stated earlier, the images reveal three types of Surtseyan activity, so the temperature results for the plume are divided into three subchapters. To interpret the temperature of the plume, a few characteristic thermal images from each type were selected and plotted together on a single graph. All profiles are drawn upward away from the vent.

To get an average temperature of the plume for each type, a single mean temperature profile, from the original data, was created.

5.1.1 Continuous uprush

Thermal images 16 to 32 are all examples of continuous uprush type of activity and all reveal similar temperature results. Thermal images (ThI) 21, 22 and 30 were used as an example. Figure 5.1 shows the images with the measurement lines and Fig. 5.2 and 5.3 show the temperature and mean temperature profiles.

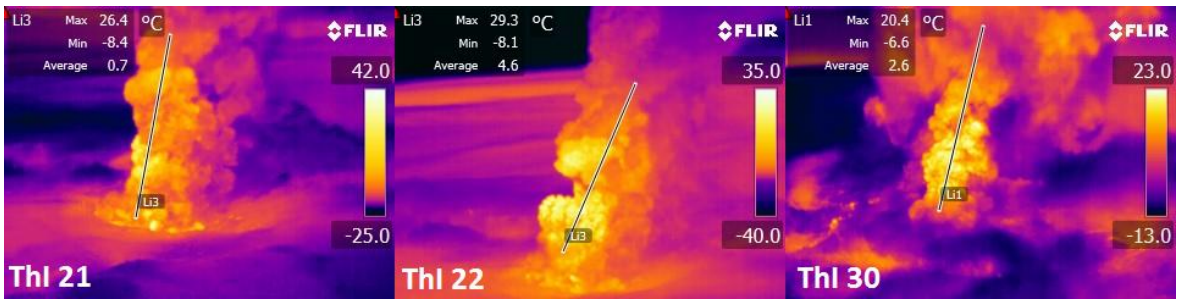

Figure 5.1: *Thermal images 21, 22 and 30 with measurement lines (Photos by Björn Oddson).*

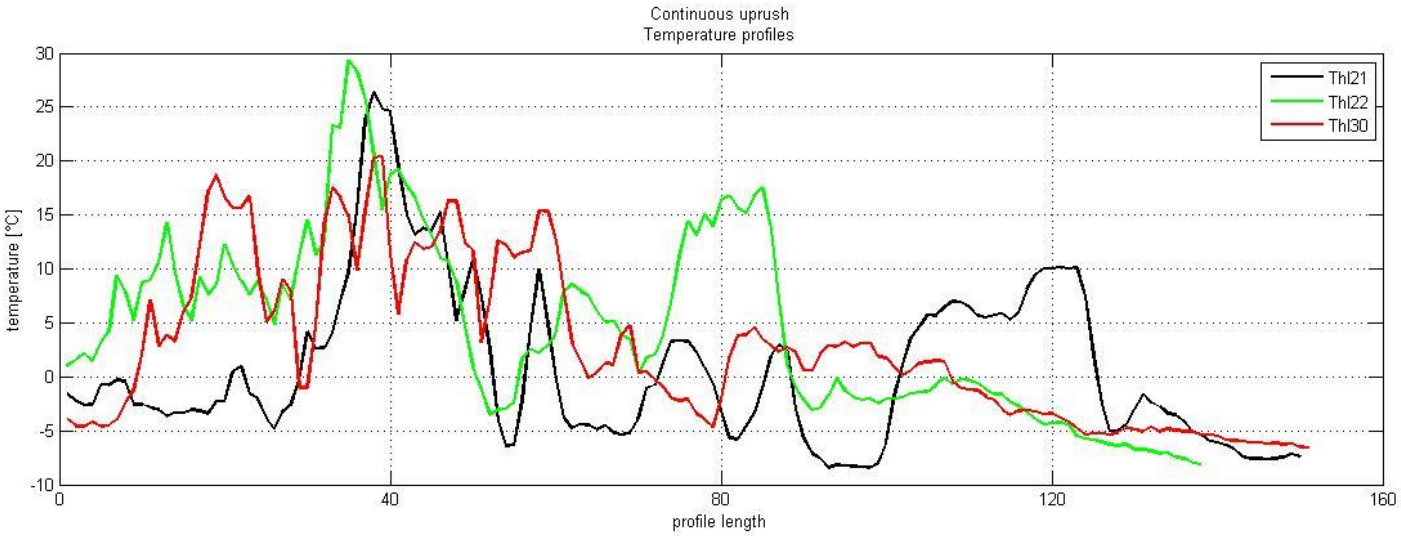

Figure 5.2: *Temperature profiles for continuous uprush activity.*

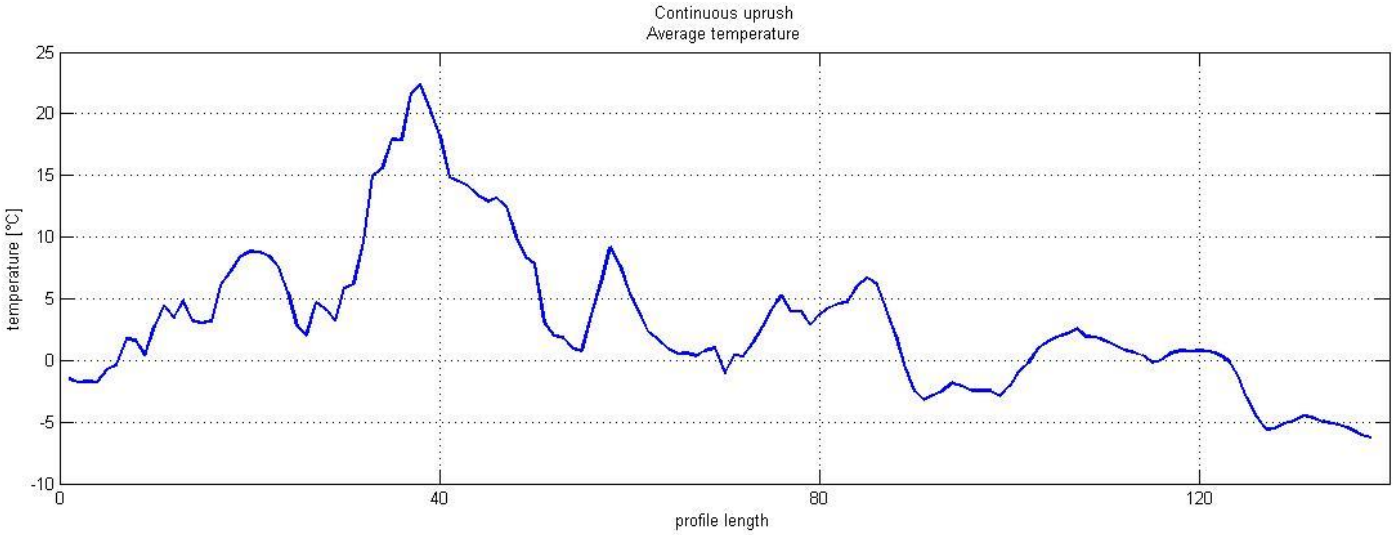

Figure 5.3: *Mean temperature profile for continuous uprush activity.*

The lengths on the graphs are not scaled but the ice cauldron, which is around 1.5 km wide from east to west, can be used as a unit of measurement. Thus, the profile for thermal image 21 is around 1.5-2 km long. As seen from Fig. 5.2 and 5.3 the highest average temperature is reached in the bottom half of the plume. After the plume has reached its highest temperature, the temperature decreases and increases alternately until it finally fades out. As the hot plume rises, cold air mixes in from the sides causing the highest temperature to remain at the top. The temperature eventually decreases due to adiabatic expansion. The reason for the increasing temperature pikes probably lies in the eruption's activity cycle. It is pushing volcanic materials up through the vent in rounds, so each pike represents the highest temperature at the top of the plume at that time.

Low clouds

Thermal images 25-29 capture approximately 5 km of low clouds expanding laterally to the SW of the crater. It's interesting to see how the temperature decreases along a horizontal line drawn through the low cloud. For an example, thermal images 26 and 27 were used. One vertical line was drawn through the center of the plume and one horizontal line through the low clouds, for each image. Figure 5.4 shows the images with the measurement lines, and figure 5.5 and 5.6 display the temperature and mean temperature profiles.

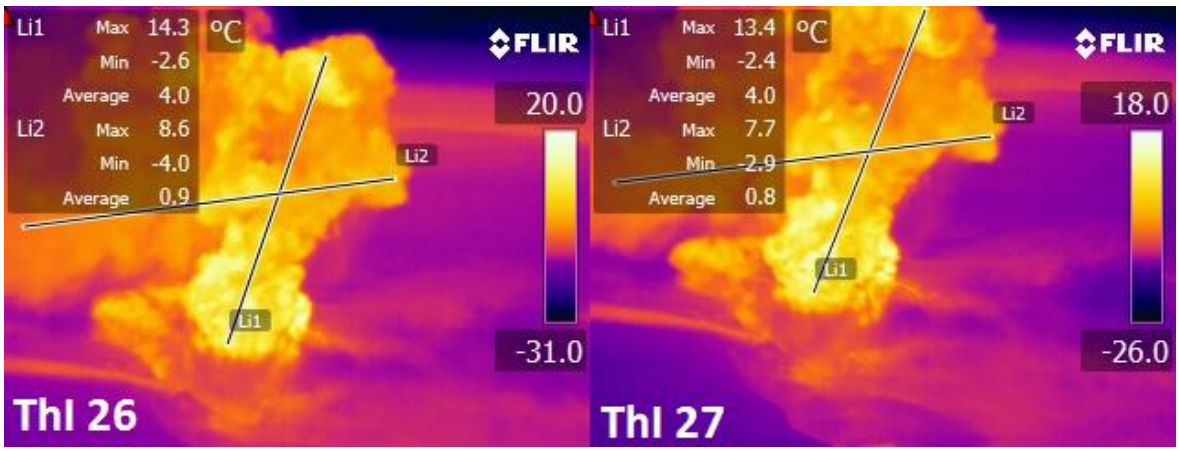

Figure 5.4: *Thermal images 26 and 27 with measurement line (Photos by Björn Oddson).*

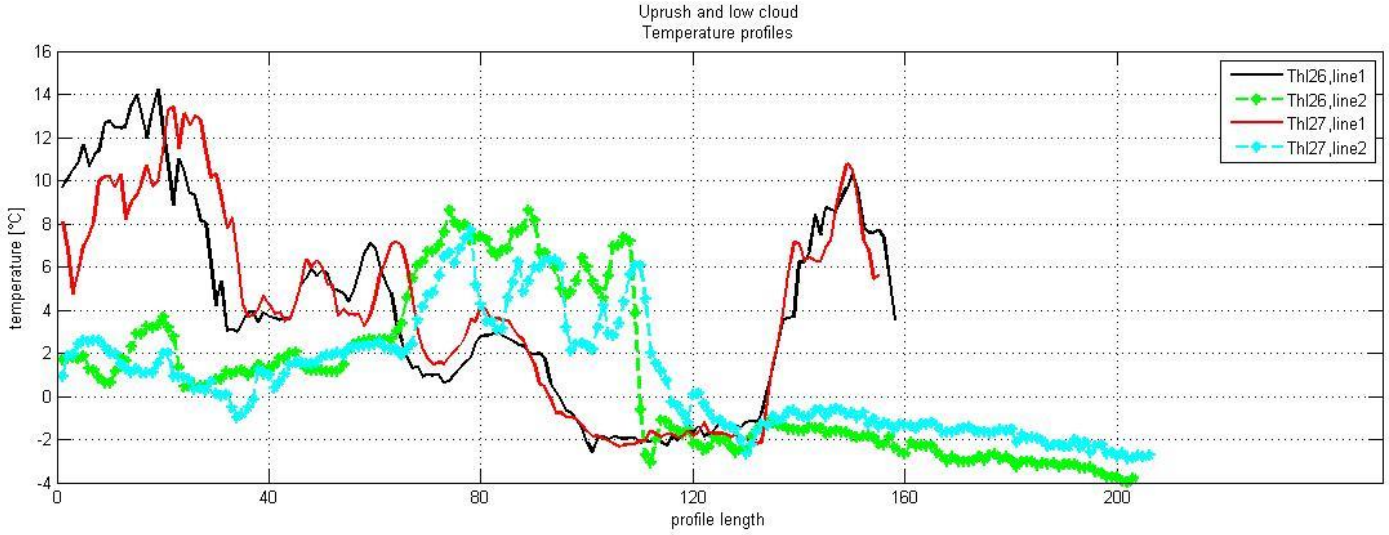

Figure 5.5: *Temperature profiles for uprush and low cloud activity.*

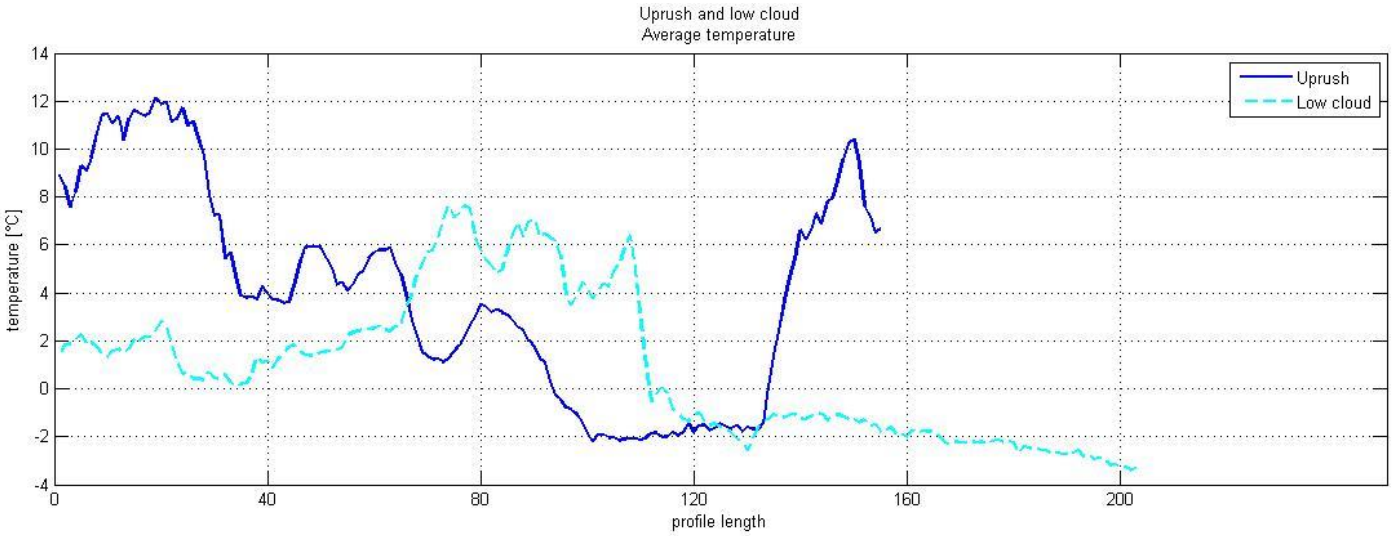

Figure 5.6: *Mean temperature profiles for uprush and low cloud activity.*

It's interesting to see how quickly the temperatures drop as the profile leaves the plume and enters the low cloud. Also, the drastic temperature increase in the plume towards the ending indicates higher temperature area inside the plume, as seen from the thermal images.

5.1.2 Continuous steaming

Thermal images 33 to 48 all reveal continuous steaming type of activity. As previously mentioned, the emissivity value for the steam plume is different than for a plume consisting of water and tephra mixture. None the less, water droplets inside the steam plume work to some extent as an emissivity surface, but the temperature values should be taken with great caution. Images 43, 46 and 47 are used as an example. Figure 5.7 shows the images with the measurement lines and figure 5.8 shows the temperature profile.

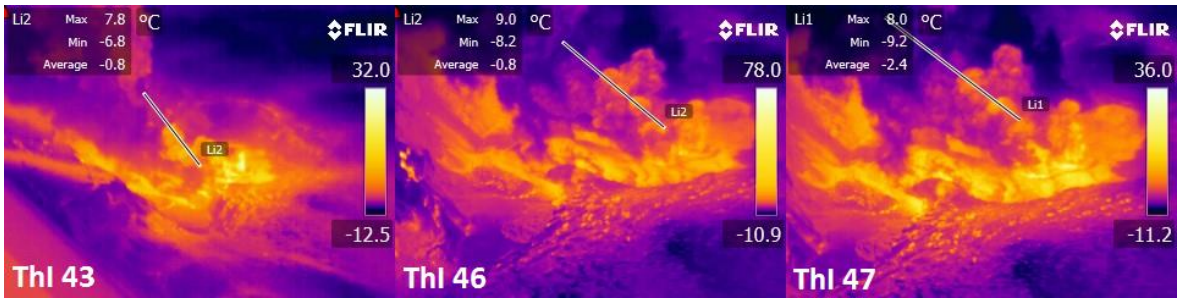

Figure 5.7: *Thermal images 43, 46 and 47 with measurement lines (Photos by Björn Oddson).*

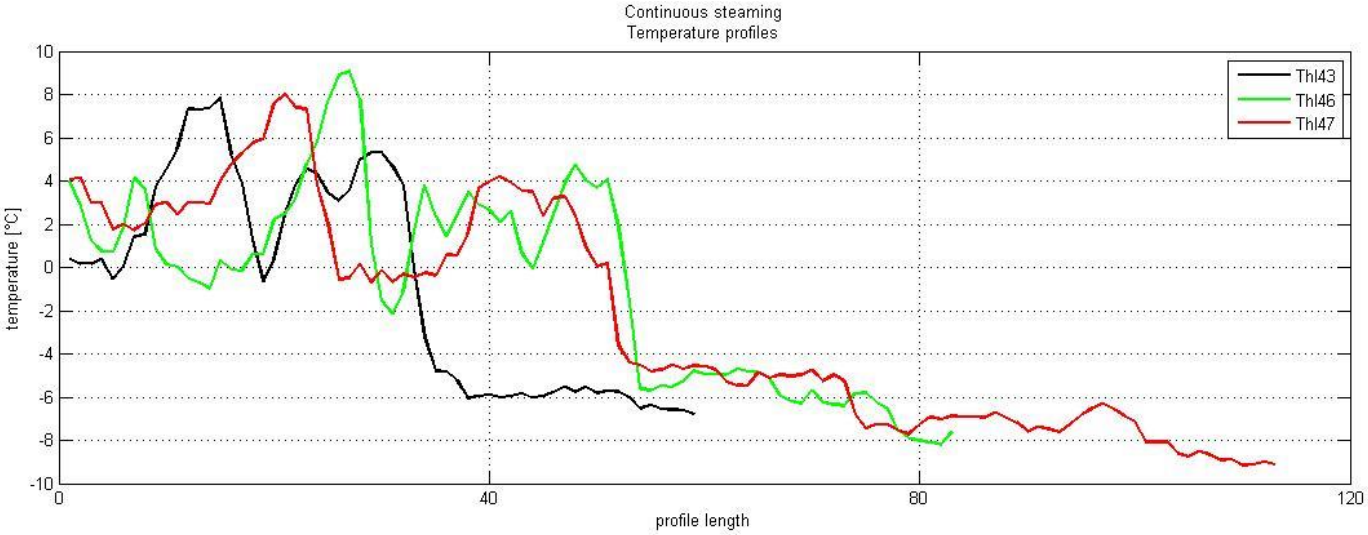

Figure 5.8: *Temperature profiles for continuous steaming activity.*

As seen from the graph, the continuous steaming type of activity produces lower temperature values than the continuous uprush. The temperature decreases rather quickly and has almost caught up with the air temperature towards the end. However, these temperature values are obtained using emissivity of 0.92, which is probably not correct for steam. The absolute numbers are therefore not to be trusted.

5.1.3 Cocktail explosions

Cocktail explosion are visible in thermal images 52-64. The temperature is expected to increase as the activity increases. For demonstration, thermal images 52, 56, 58 and 62 were examined. Figure 5.9 shows the images and measurement lines and figure 5.10 displays the temperature profiles.

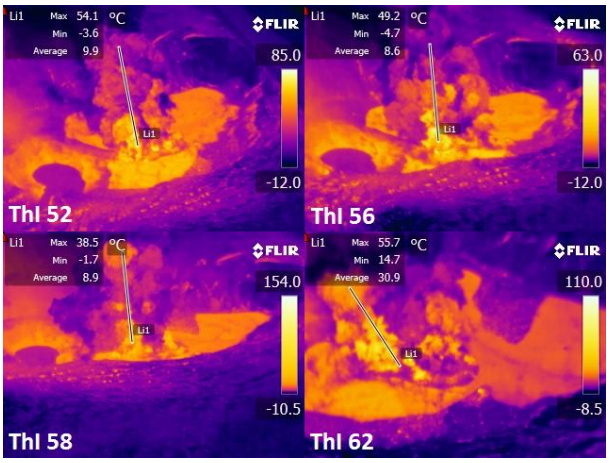

Figure 5.9: *Thermal images 52, 56, 58 and 62 with measurement lines (Photos by Björn Oddson).*

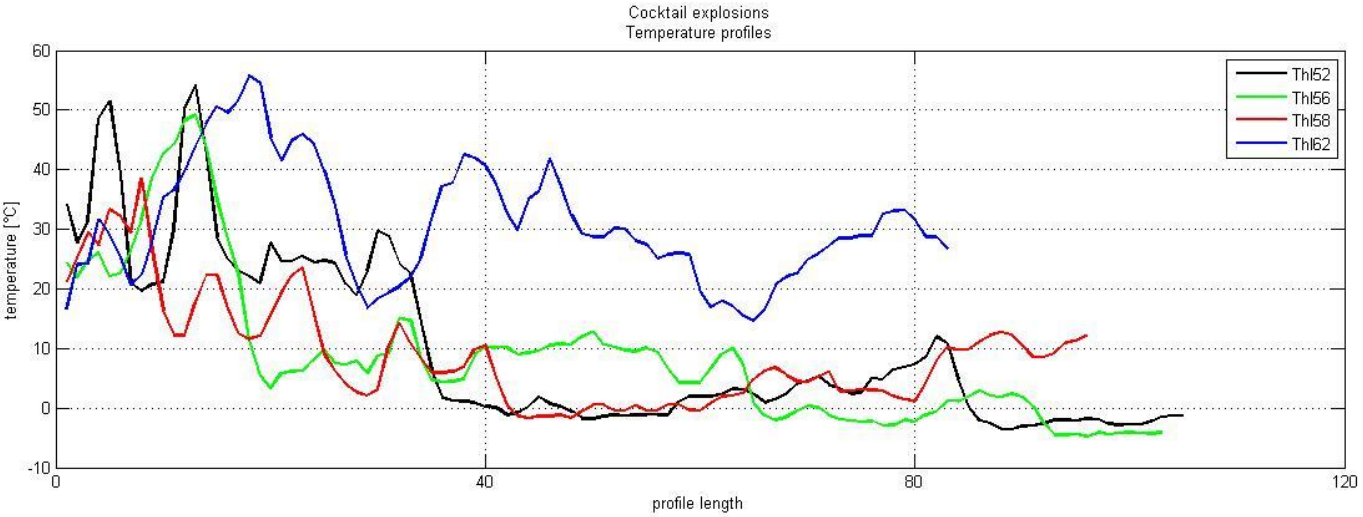

Figure 5.10: *Temperature profiles for cocktail explosions activity.*

As expected so close to the vent, the temperature values are much higher than in the uprush or steam examples. The explosions are only minor and the lava bombs land close to the vent. As a result, the temperature quickly decreases as the plume rises, reaching similar temperature values as the continuous uprush activity.

5.2 Crater

The crater's rim is visible on various thermal images. Images 48, 56 and 58 provide very nice viewing angle of the rim so they are used here for temperature measurements. Figure 5.11 shows the images and measurement lines and Figure 5.12 displays the temperature profile.

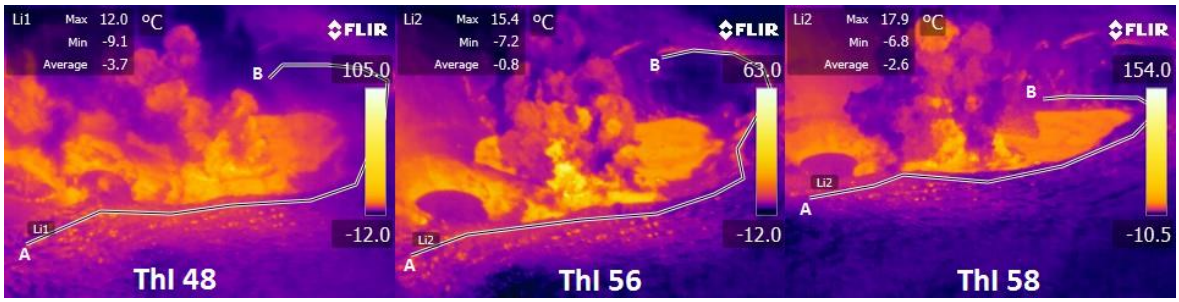

Figure 5.11: *Thermal images 48, 56 and 58 with measurement lines (Photos by Björn Oddson).*

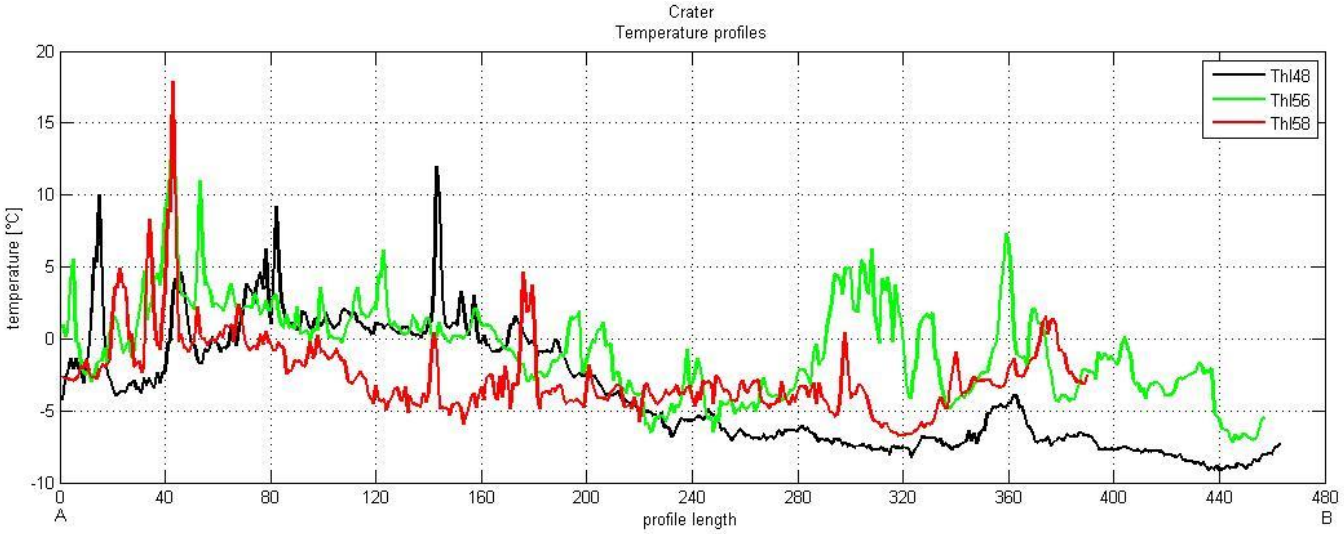

Figure 5.12: *Temperature profiles for the crater.*

The highest temperature for the crater is 17,9°C, obtained on the NE side, but mostly its temperature is below zero.

5.3 Crater lake

The last four thermal images (61, 62, 63, and 64) capture very clearly the crater lake. The lake can be divided into three areas, area A, B and C (fig 5.13) and thermal images 62, 63 and 64 were used as an example.

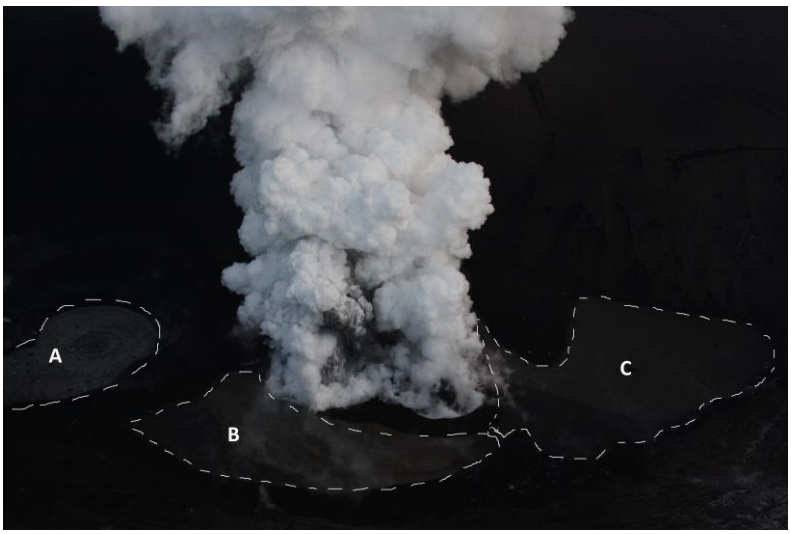

Figure 5.13: *Areas division for the lake.*

One line was drawn through area B and two lines, vertical and horizontal, were drawn through area C. One line was drawn through area A in thermal image 64. Figure 5.14 shows the images with the measurement lines and figure 5.15 and 5.16 display the temperature and mean temperature profiles.

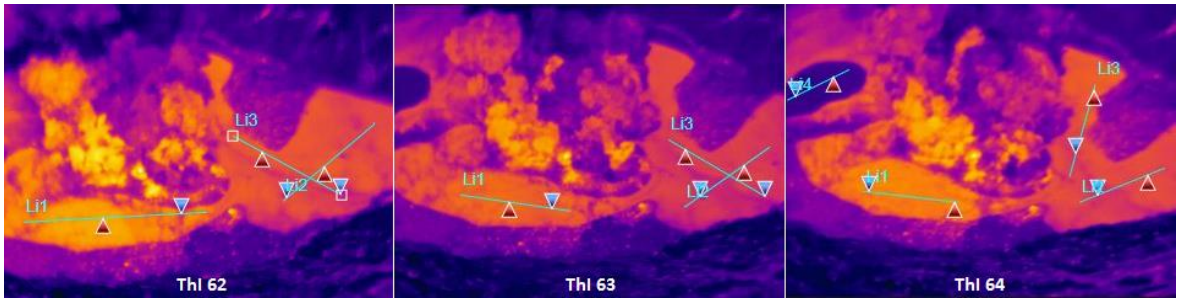

Figure 5.14: *Thermal images 62, 63 and 64 and measurement lines. Red triangles mark the hottest temperature along each line and blue triangles mark the coldest temperature.*

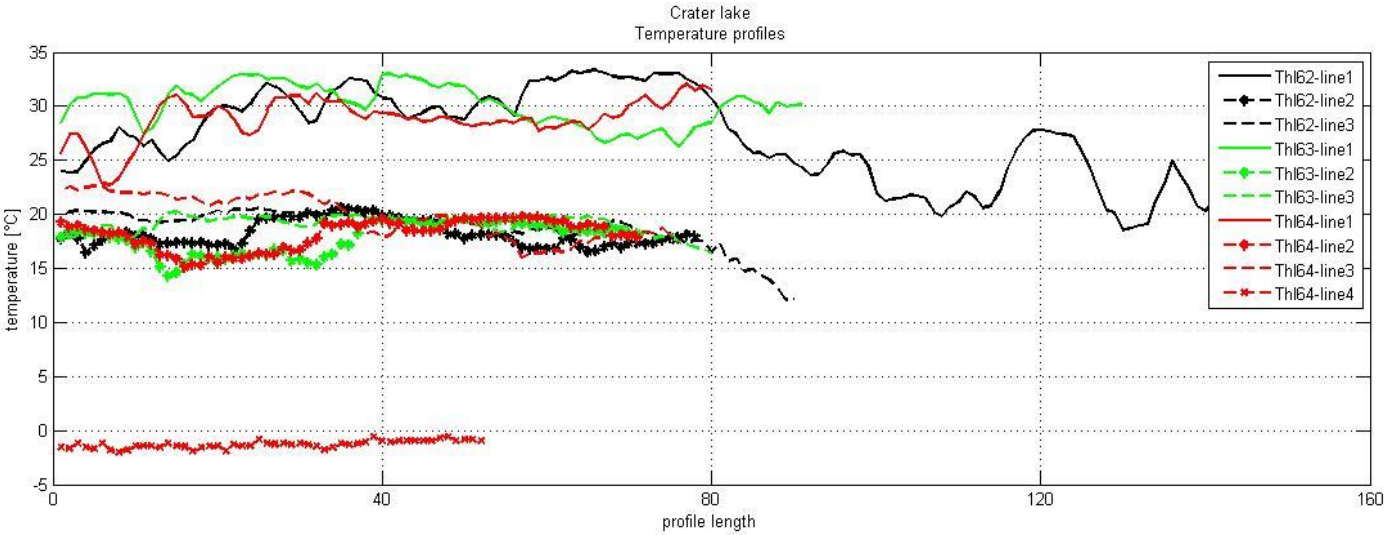

Figure 5.15: *Temperature profiles for the crater lake.*

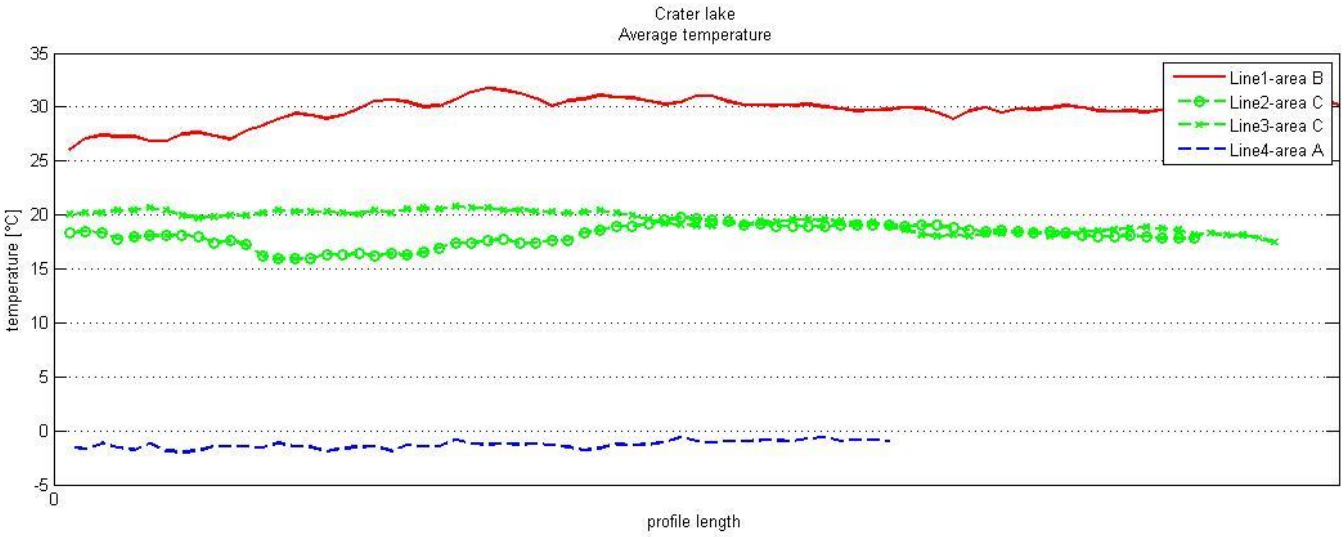

Figure 5.16: *Mean temperature profiles for the lake. Red line marks area B, green lines area C and blue line area A.*

The two graphs reveal very clearly the temperature distribution of the lake. Area B is around 12°C hotter than area C, so the activity must be stronger in that area. It's interesting that area A is just under 0°C, which indicates a minor temperature error (because water cannot be below 0°C unless frozen). However, photographs do reveal small chunks of ice floating on the water surface so actual temperature for area A is probably very close to 0°C, with error of only few degrees (Magnús Tumi Guðmundsson, pers. com.).

5.3.1 Higher temperatures

Some images revealed very high temperatures around the vent opening. The camera's object range was only between -20°C to 120°C but the camera is still able to detect higher temperature, only with less accuracy. Thermal images 52, 53, 62 and 63 all display high temperature values and are used as an example. Horizontal line was drawn through the highest temperature across the vent. Figure 5.17 shows the images where the red triangles show the hottest spot in the image. Figure 5.18 displays the temperature profiles for these images.

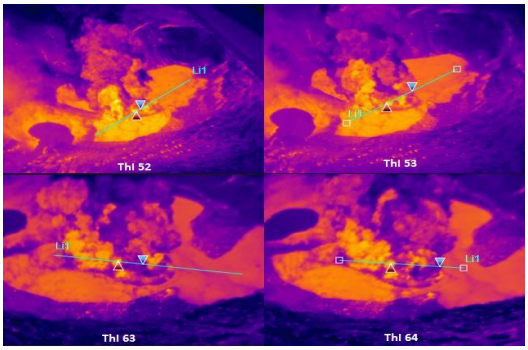

Figure 5.17: *Thermal images 52, 53, 63 and 64. Red triangles mark the hottest spot in each image (Photos by Björn Oddson).*

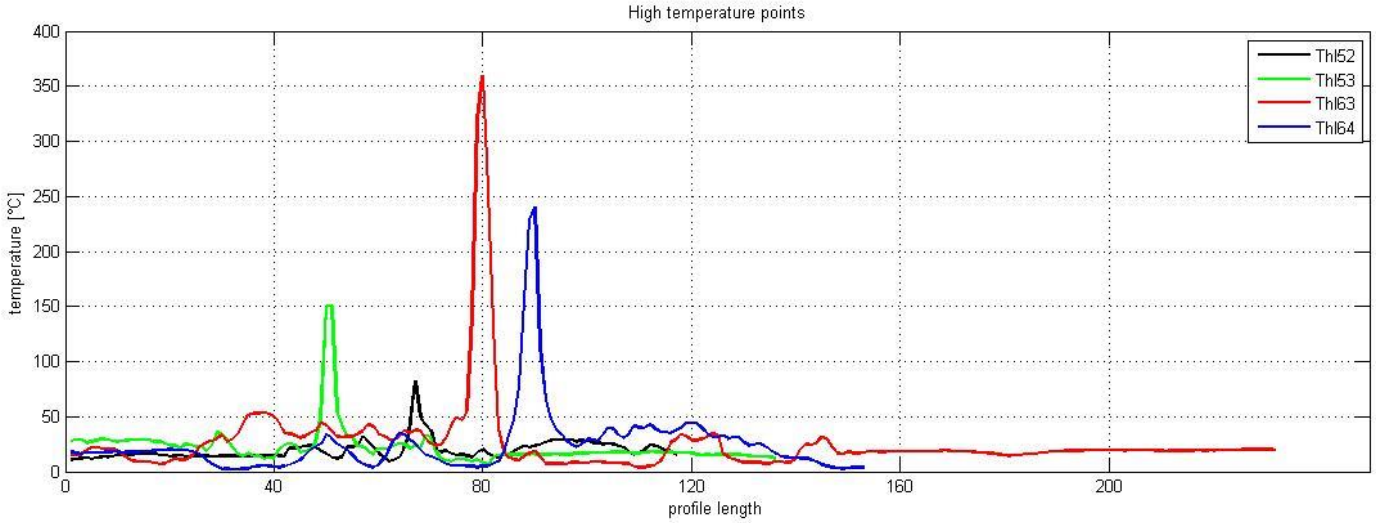

Figure 5.18: *Temperature profiles across the highest temperature across the vent.*

The highest temperature of all the thermal images is 360.2°C, obtained in image 63.

6 DISCUSSION

The temperature profiles reveal how the plume temperature changes through different stages of activity. For the continuous uprush the plume's temperature is around 20°C to 30°C before it starts to decrease further away from the vent. As the volcanic material decreases and the plume enters continuous steaming activity the plume temperature decreases down to around 7°C to 10°C. At this point the activity is very weak, so the steam both represents low activity and the importance of tephra particles for the temperature of the plume. As the activity increases and cocktail explosions appear, the temperature sharply increases to >40°C. It's interesting to see such a distinctive difference between the different activities and how radically the plume changes in such a short time.

The crater's rim and crater lake reveal more coherent results, and the observed temperature values can be expected to be close to the true values, because they work much better as a surface for the emissivity. The crater reaches its highest temperature, 5°C to 15°C, at the NE side but the average temperature of -6°C to -8°C is closer to the surface temperature. The results for the crater lake show very distinctly the temperature variation in the lake. Area B, with temperature of around 25°C to 35°C, is closest to the vent and under most influence from the heat. Area C is slightly colder with temperature around 15°C to 20°C indicating less activity in that area. For area A, which has apparent temperature just below zero, it's obvious the heat doesn't have much influence.

Compared to other examples of infrared thermal monitoring, Grímsvötn has very low temperatures. FLIR measurements in Stromboli in 2001-2004 reveal temperature values from 150°C to over 300°C (Patrick et a. 2007). Similar, in Mount St. Helens in 2004 thermal imaging reveals temperature values as high as 700°C (Schneider et al. 2008). The difference between these examples and the reason for Grímsvötn low temperature values is the watery environment. A lot of energy is needed to boil external waters, but total cooling effects from the melting, water heating and the evaporation is the main cause for lower temperature values in Grímsvötn eruption plumes compared to plumes in areas with no water.

It would have been interesting to have thermal data from more than just one day at Grímsvötn for comparison and further monitoring. None the less, thermal imaging gave good, exact data which can be compared with the data from next time Grímsvötn erupts.

REFERENCES

Ball, M. and Pinkerton, H. 2006. Factors affecting the accuracy of thermal imaging cameras in volcanology. *J. Geophys. Res.* 111, B11203, doi:10.1029/2005JB003829.

FLIR. 2008. *User's manual, FLIR R&D software 3.3*

FLIR. *2008. The ultimate infrared handbook for R&D professionals.*

Guðmundsson, M.T. 2005. Subglacial volcanic activity in Iceland. *In* Caseldine, C.J., Russel, A., Harðardóttir, J. and Ó. Knudsen, eds. *Developments in Quaternary Science; 5. Iceland: Modern processes, Past Environments* Elsevier, 127-151

Gudmundsson, M.T., Á. Höskuldsson, G. Larsen, T. Thordarson, B.A. Oladottir, B. Oddsson, J. Gudnason, T. Högnadottir, J.A. Stevenson, B.F. Houghton, D. McGarvie, and G.M. Sigurdardottir *The May 2011 eruption of Grímsvötn*. Abstract, EGU General Assembly.

Harris, A. 2013. *Thermal remote sensing of active volcanoes. A user's manual.* New York: Cambridge University Press.

Hreinsdóttir, S., Sigmundsson, F., Roberts, M.J., Björnsson, H. Grapenthin, R., Arason, Th., Árnadóttir, Th., Hólmjárn, J., Geirsson, H., Bennett, R.A., Guðmundsson, M.T., Oddsson, B., Ófeigsson, B.G., Villemin, T., Jónsson, Th., Sturkell, E., Höskuldsson, Á., Larsen, G., Thordarson, Th. and Óladóttir, B.A. 2014. Volcanic plume height correlated with magma-pressure change at Grímsvötn Volcano, Iceland. *Nature geoscience* 7, 214-218

Jakobsdóttir, S.S., Roberts, M.J., Guðmundsson, G.B. and Holmjarn, J. 2011. Volcanic eruption in Grímsvötn, 21 May 2011. *In* Neuberg, J., Carniel, R., Falsaperla, S. and Langer H., eds. *S.O.S.: Seismic and other signals; Abstract volume. September 17 to 24, Salina, Aeolian Isalnds, Italy.* INGVCT2011-025

Jakobsson, S.P. and Guðmundsson, M.T. 2008. Subglacial and intraglacial volcanic formations in Iceland. *Jökull* 58, 179-196

Jude-Eton, T.C., Thordarson, T. and Guðmundsson, M.T. 2012. Dynamics, stratigraphy and proximal dispersal of supraglacial tephra during the ice-confined 2004 eruption at Grímsvötn Volcano, Iceland. *Bull Volcano* 74, 1057-1082

Larsen, G., Guðmundsson, M.T. and Björnsson, H. 1998. Eight centuries of periodic volcanism at the center of the Iceland hotspot revealed by glacier tephrostratigraphy. *Geology* v.26, 943-946.

Mikron Infrared, Inc. 2006. *MikroScan 7600PRO Thermal Images Operator's Manual*. Oakland, USA. 275-286.

Patrick, M.R., Harris, A.J.L, Ripepe, M., Dehn, J., Rothery, D.A. and Calvari S. 2007. Strombolian explosive styles and source conditions: insights from thermal (FLIR) video. *Bull Volcano* 69, 769-784

Schneider, B.J., Wallence, J.W., Wessels, R.L., Logan, M. and Ramsey, M.S. 2008. Use of thermal infrared imaging for monitoring renewed dome growth at Mount St. Helens, 2004. *In* Sherrod, D.R., Scott, W.E. and Stauffer, P.H, eds. *A volcano rekindled; the renewed eruption of Mount St. Helens, 2004-2006,* 347-361

Stewart, S.F., Pinkerton, H., Blackburn G.A. and Guðmundsson, M.T. 2008. Monitoring active subglacial volcanoes: a case study using airborne remotely sensed imagery of Grímsvötn, Iceland. *International journal of remote sensing* 29 (22), 6501-6514

White, J.D.L. and Houghton, B. 2000. Surtseyan and related phreatomagmatic eruptions. *In* Sigurðsson, H, ed. *Encyclopedia of Volcanoes.* 495-513.

Young, H.D. and Freedman, R.A. 2011. *University physics with modern physics, volume 2* (Thirteen ed.). Milan: Rotolito Lombarda SpA, pp. 1051-1055

Appendix

A Thermal Images

16 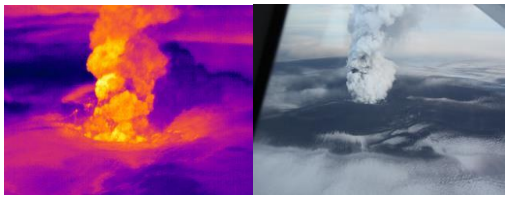

IR_2816.jpg and 2011-05-24MTG79

17 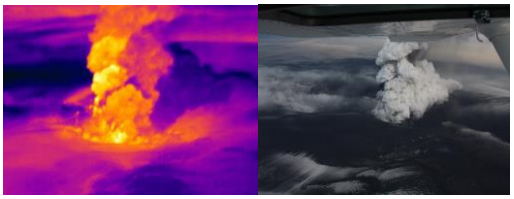

IR_2817.jpg and 2011-05-24MTG80

19 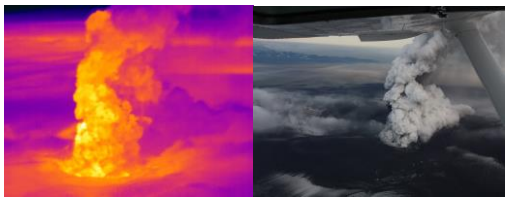

IR_2819.jpg and 2011-05-24MTG81

20 

IR_2820.jpg and 2011-05-24MTG82

21 

IR_2821.jpg and 2011-05-24MTG86

22 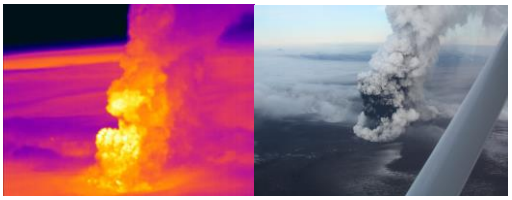

IR_2822.jpg and 2011-05-24MTG88

23 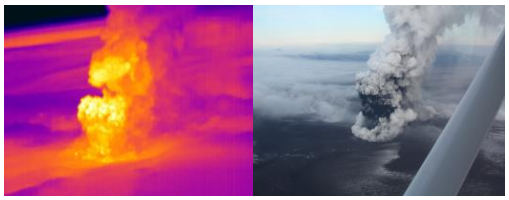

IR_2823.jpg and 2011-05-24MTG88

25 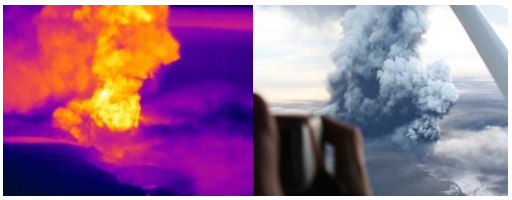

IR_2825.jpg and 2011-05-24MTG137

26 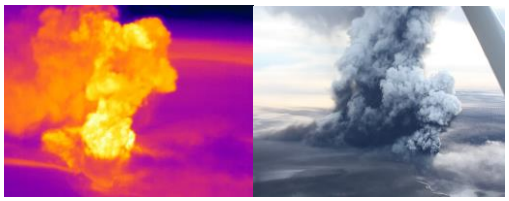

IR_2826.jpg and 2011-05-24MTG138

27 

IR_2827.jpg and 2011-05-24MTG139

28 

IR_2828.jpg and 2011-05-24MTG150

29 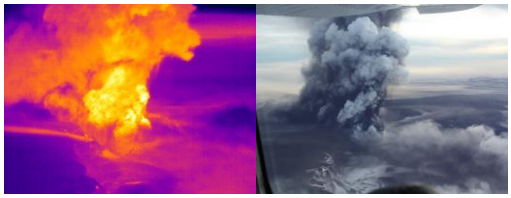

IR_2829.jpg and 2011-05-24MTG151

30 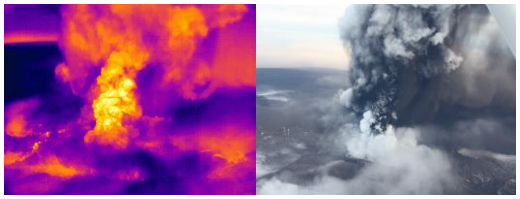

IR_2830.jpg and 2011-05-24MTG152

31 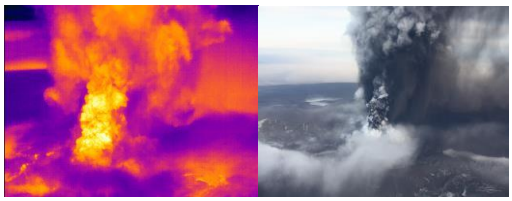

IR_2831.jpg and 2011-05-24MTG156

32 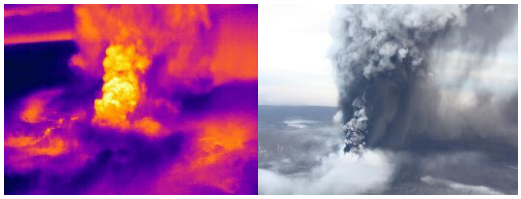

IR_2832.jpg and 2011-05-24MTG157

33 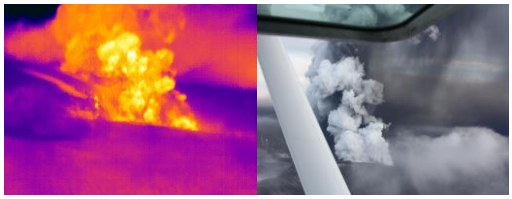

IR_2833.jpg and 2011-05-24MTG176

34 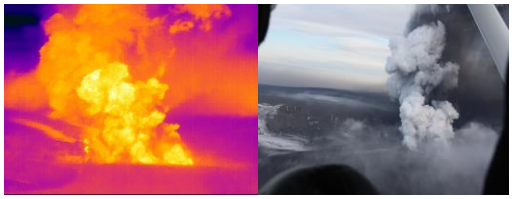

IR_2834.jpg and 2011-05-24MTG179

36 

IR_2836.jpg and 2011-05-24MTG180

37 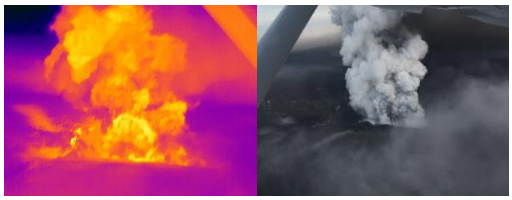

IR_2837.jpg and 2011-05-24MTG181

38 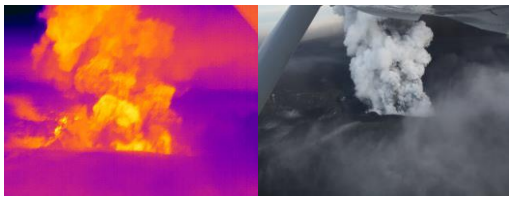

IR_2838.jpg and 2011-05-24MTG182

39 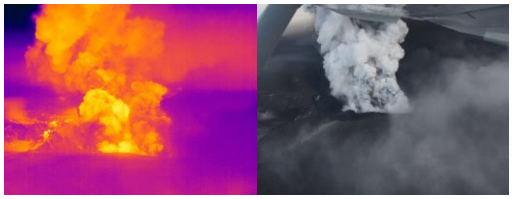

IR_2839.jpg and 2011-05-24MTG183

40 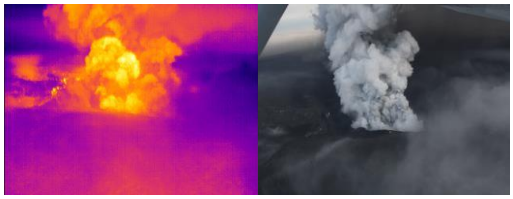

IR_2840.jpg and 2011-05-24MTG184

41 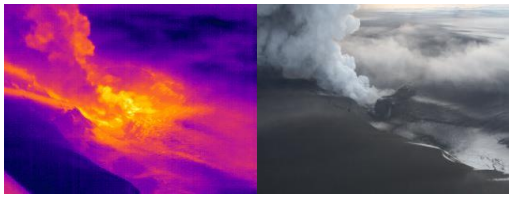

IR_2844.jpg and 2011-05-24MTG205

42 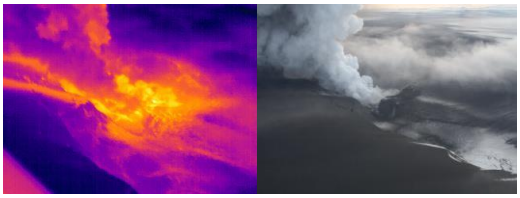

IR_2842.jpg and 2011-05-24MTG205

43 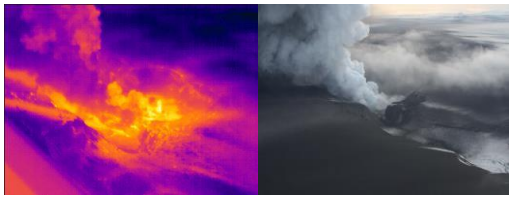

IR_2843.jpg and 2011-05-24MTG206

44 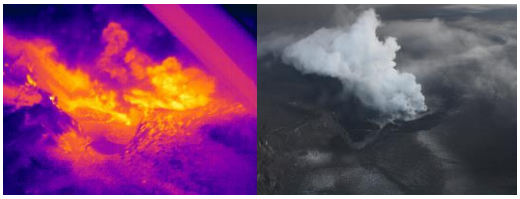

IR_2844.jpg and 2011-05-24MTG218

46 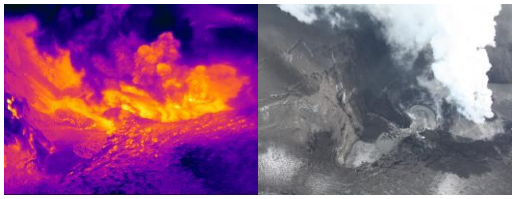

IR_2846.jpg and 2011-05-24MTG229

47 

IR_2847.jpg and 2011-05-24MTG230

48 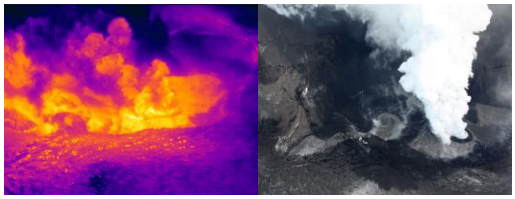

IR_2848.jpg and 2011-05-24MTG232

52 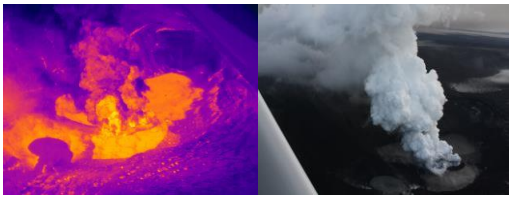

IR_2852.jpg and 2011-05-24MTG245

53 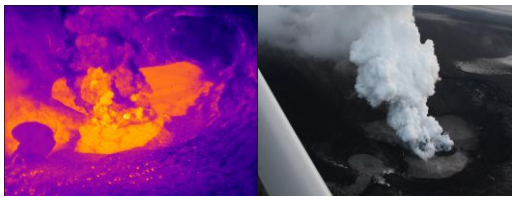

IR_2853.jpg and 2011-05-24MTG246

54 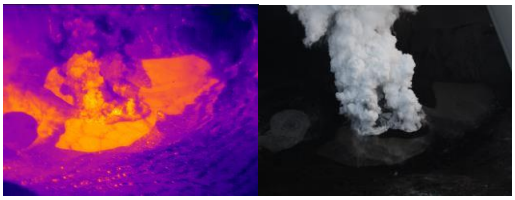

IR_2854.jpg and 2011-05-24MTG247

56 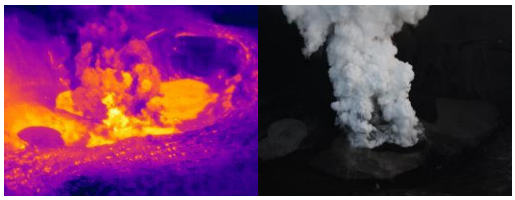

IR_2856.jpg and 2011-05-24MTG287

57 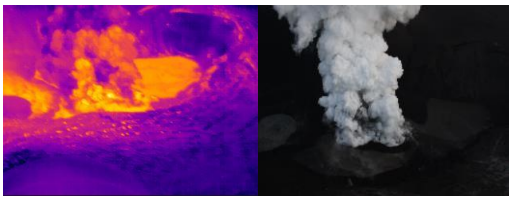

IR_2857.jpg and 2011-05-24MTG288

58 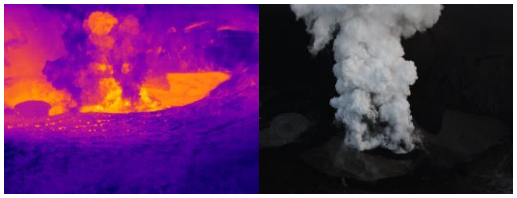

IR_2858.jpg and 2011-05-24MTG289

61 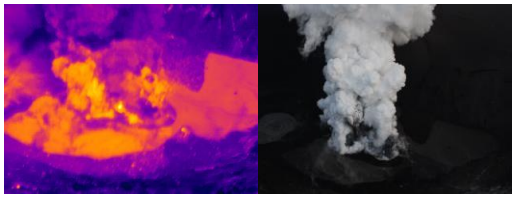

IR_2861.jpg and 2011-05-24MTG290

62 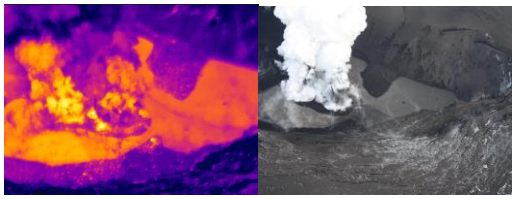

IR_2862.jpg and 2011-05-24MTG291

63 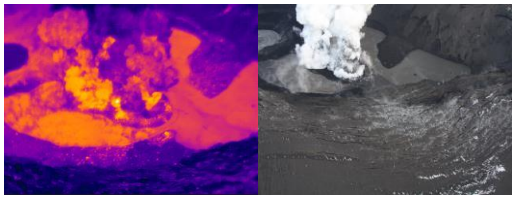

IR_2863.jpg and 2011-05-24MTG292

64 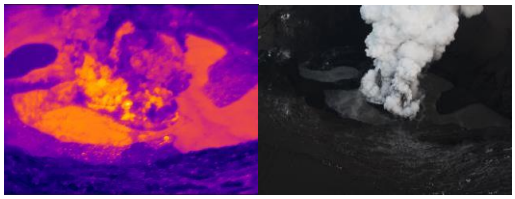

IR_2864.jpg and 2011-05-24MTG293